Analysis of rectangular resonant cavities in terahertz parallel-plate waveguides

Victoria Astley, Blake McCracken, Rajind Mendis, and Daniel M. Mittleman*

Department of Electrical and Computer Engineering, Rice University, MS 366, Houston, Texas 77251-1892, USA
**Corresponding author: daniel@rice.edu*

Received February 14, 2011; revised March 17, 2011; accepted March 20, 2011;
posted March 21, 2011 (Doc. ID 142628); published April 14, 2011

We describe an experimental and theoretical characterization of rectangular resonant cavities integrated into parallel-plate waveguides, using terahertz pulses. When the waveguide is excited with the lowest-order transverse-electric mode, these cavities exhibit resonances with narrow linewidths. Broadband transmission spectra are compared with the results of mode-matching calculations, for various cavity dimensions.

OCIS codes: 230.7370, 230.5750, 300.6495.

Optical sensing technologies often rely on engineered resonant structures for the detection and identification of materials. The application of this concept to sensing in the terahertz regime has grown as an area of research, leading to the development of a variety of resonant structures for different sensing applications. Many designs have been studied at terahertz frequencies, such as dielectric fiber-based sensors [1,2], photonic crystal structures and cavities [3–5], corrugated waveguides [6,7], metallic meshes [8], and split-ring resonators [9–11]. There have also been several designs that employed resonant structures embedded within parallel-plate waveguides (PPWGs), such as Bragg gratings and photonic band gap structures [12–14]. These latter examples have all employed the transverse electromagnetic mode of the PPWG, which provides low-loss and low-dispersion propagation of terahertz waves [15].

With the recent investigation of the lowest-order transverse-electric (TE_1) mode of the PPWG [16,17], a simpler resonant cavity geometry was proposed: a rectangular groove machined into one inner face of the waveguide, oriented perpendicular to the direction of propagation [see Fig. 1(a)]. Despite the simplicity of this cavity, the resulting resonance has a strong extinction and its line width is among the narrowest ever reported in the terahertz range for an artificial structure [16]. The narrow line width is advantageous for increased sensitivity, due to the smaller minimum detectable frequency shift. This design has been implemented as a highly sensitive microfluidic sensor, in which small changes in the refractive index of a liquid filling the rectangular groove could be measured [18]. In these previous experiments, the results were compared with finite element method simulations. As a first approach, numerical simulations provided accurate results, but in order to fully understand the operating principle and underlying physics of the cavity, as well as to make the most effective use of its sensing possibilities, a theoretical explanation is required.

The resonance frequency and line width are clearly dependent on the geometry of the cavity, but the nature of that dependence is not known. Simple explanations such as modeling the cavity as a one- or two-dimensional (2D) rectangular standing-wave resonator do not agree with experimental observations or the results of numerical simulations, indicating that a more complex analytical framework is required. To build a quantitative understanding of the relationship between the cavity geometry and its resonant behavior, here we present a thorough theoretical and experimental study.

First, we obtain experimental data on the resonant behavior of cavities with a range of various rectangular geometries. Several waveguides were fabricated from polished aluminum plates, each with a rectangular groove machined into one plate to serve as the resonant cavity. The cavity geometries were designed in two sets: one set with a constant depth ($406 \pm 5\,\mu$m) but varying widths, and one set with a constant width ($460 \pm 5\,\mu$m) but varying depths. The waveguide propagation lengths were all the same, 5.9 mm, and the cavities were centered midway between the entrance and exit facets. We assemble the plates with dielectric spacers fixing the separation at 1 mm ($\pm 5\,\mu$m).

To measure the frequency-dependent transmission spectra, we use a conventional pulsed terahertz time-domain spectrometer based on photoconductive antennas [19]. The incident broadband radiation is weakly focused onto the input facet. The electric field of the incident beam is oriented parallel to the plates in order to excite the TE modes of the PPWG. The radiation emerging from the output end of the waveguide is collected, and time-domain waveforms are measured with an extended time window (1.6 ns) to achieve high spectral resolution (~0.6 GHz). Transmission spectra are obtained by Fourier transform. A PPWG without an integrated

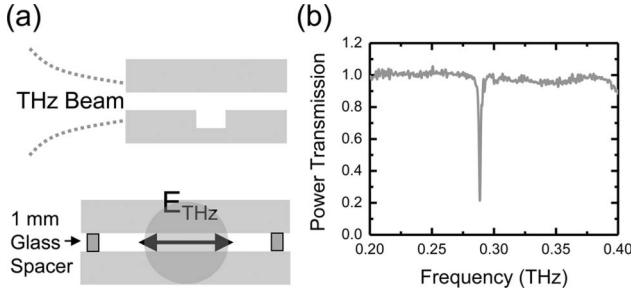

Fig. 1. (a) Longitudinal cross section (top) and input face view (bottom) of the assembled PPWG (not to scale). (b) A typical power transmission spectrum for a PPWG with a 400 μm wide by 406 μm deep groove, showing the dominant resonant feature characteristic of this cavity geometry.

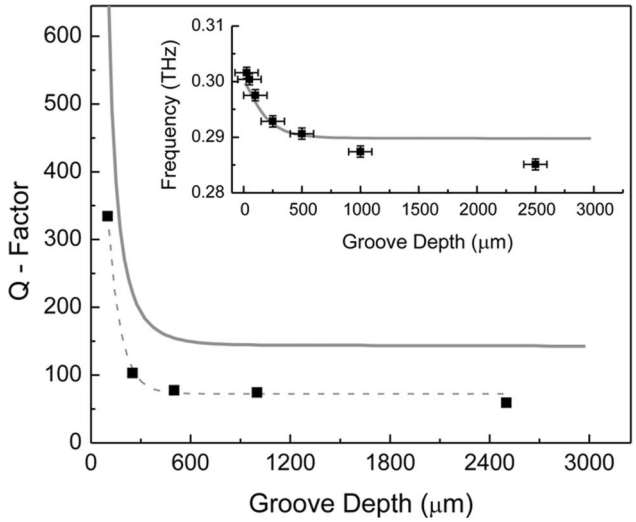

Fig. 2. Q factor and resonant frequency (inset) produced by rectangular grooves of 460 μm width and varying depth. Experimental data (squares) are compared to the results of mode-matching analysis (gray curves).

cavity serves as the reference. A typical transmission spectrum [as in Fig. 1(b)] contains one dominant feature: a resonant dip. This feature shifts to higher frequencies as the depth of the groove decreases for a fixed width (Fig. 2). As shown in Fig. 2, this increase in the resonant frequency corresponds to an increasing quality (Q) factor, with a maximum observed Q of 334 for the groove with 100 μm depth. Grooves shallower than 100 μm produce resonant dips with lower extinction, which allow accurate determination of the center frequency but not the line width. The observed trend, with shallower cavities yielding higher frequencies and narrower resonances (not shown here), is intuitive as it agrees qualitatively with the simple model of a rectangular standing-wave resonator. However, the agreement is only qualitative—an attempt to predict the resonant frequency using this analytic model produces inaccurate results. For example, for a groove of width $w = 460\,\mu$m and depth $h = 1000\,\mu$m, a standing-wave analysis predicts a resonant frequency of

$$f_R = \frac{c}{2}\sqrt{\left(\frac{1}{w}\right)^2 + \left(\frac{1}{h}\right)^2} = 359\,\text{GHz},$$

(for a first-order 2D cavity resonance), whereas the experimental result for this set of geometrical parameters is $f_R = 287.4$ GHz.

In contrast to those of the cavities of varying depth and constant width, the experimental spectra for cavities of varying width and constant depth show a more complicated dependence on geometry. As the groove widens, the dominant resonance dip red shifts, while it also broadens the widths up to about 790 μm. Beyond this width, additional resonant features appear, indicating the excitation of higher-order cavity modes (see Fig. 3). Several of these features exhibit high Q values of above 100, and some exhibit marked asymmetry. The lack of an obvious trend for these resonant features complicates the attempt to quantify the dependence on geometry.

To understand this complex behavior, we use a mode-matching analysis based on classical waveguide theory [13,20–24]. In this approach, the "cavity area" is treated as a PPWG section with a different plate separation. The composite waveguide can then be analyzed sequentially, by propagation within waveguide sections and abrupt (virtual) junctions between waveguide sections with different plate separations. At the two junctions (i.e., the start and end of the cavity area), we compute scattering matrices that express the electromagnetic energy reflected and transmitted into various TE modes. For example, a TE_1 mode propagating in the first (input) waveguide section, arriving at the first junction, may couple into any TE_n mode of the cavity area, and may reflect into any TE_m mode of the first waveguide section $(n, m = 1, 3, 5, \ldots)$. The coupling coefficients are calculated from the spatial overlap between the relevant mode patterns. The scattering matrices at each junction and the propagation matrices for the uniform waveguide sections are combined to generate a single transmission matrix, which can be used to calculate the transmission and reflection coefficients of incident waves at any frequency.

When we apply this method to an incident single TE_1 mode wave and consider only the TE_1 component of the output, we obtain excellent agreement in the power transmission spectra corresponding to experiment and theory (Fig. 3), up to 450 GHz. At this frequency, we reach the cutoff frequency of the TE_3 mode. Above this frequency, the input is most probably still single (TE_1) mode [16,17], but the output is probably not. Therefore, to match the theoretical spectra to the experimental ones, we would need to expand the analysis to consider TE_3 mode propagation at the output. For grooves of varying depth, the predicted resonant frequencies from

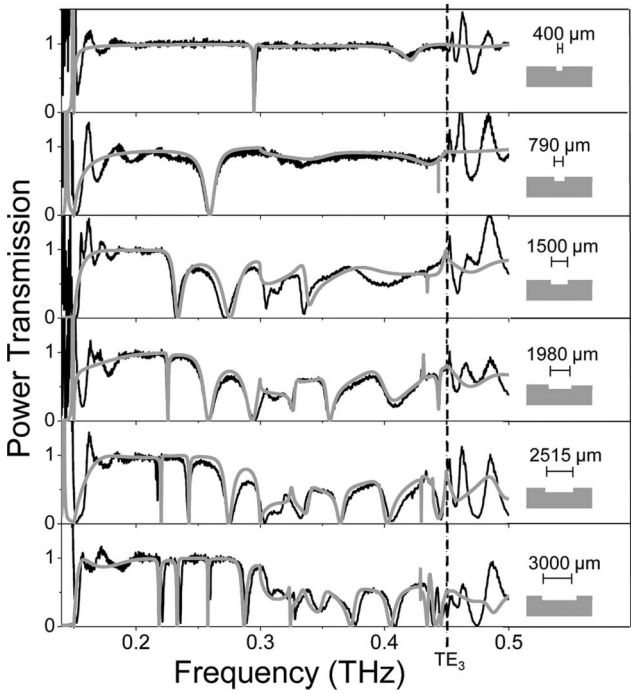

Fig. 3. Power transmission spectra from PPWGs with rectangular grooves of 406 μm depth and varying width. The width of each groove and a sketch of the waveguide geometry are given to the right of each spectrum. The black dotted line marks the TE_3 cutoff frequency.

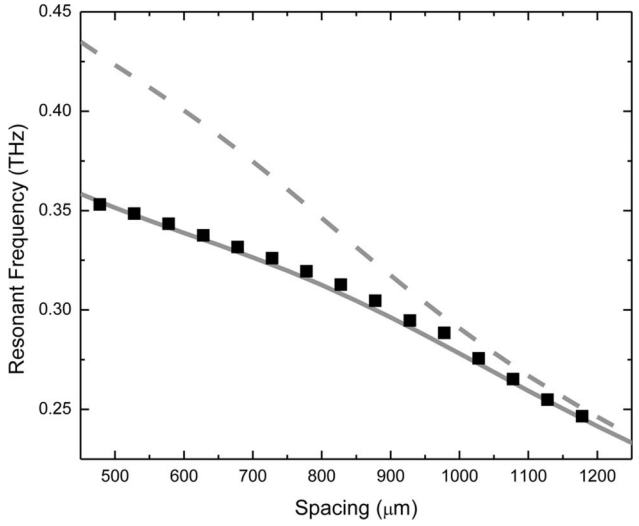

Fig. 4. Resonant frequency versus PPWG plate separation. As the spacing between waveguide plates decreases, the dominant resonant feature shifts to higher frequencies. Comparison of experimental results (black squares) to results from FEM simulation (solid gray curve) and mode-matching analysis (dotted gray curve).

mode-matching analysis are also in reasonably good agreement with the experiment (Fig. 2). The mode-matching analysis also accurately predicts the trend in the cavity Q, with the overestimation of the Q values probably resulting from losses in the cavity and imperfections in the fabrication.

As a final experimental test, we place a waveguide with a single groove of 412 μm deep by 460 μm wide in an experimental arrangement that continuously varies the waveguide plate separation. In this configuration, we observe a resonant dip that gradually red shifts with increasing plate separation (Fig. 4). A mode-matching analysis (dashed curve) predicts the general trend accurately, though its accuracy decreases for smaller plate separations, probably due to the increasingly abrupt effective change in plate spacing at the cavity junction. Also, as the plate spacing decreases, the resonant frequency gradually approaches the cutoff frequency of the TE_1 mode (which itself increases as the spacing narrows) until the resonance becomes undetectable. Results from a finite element method (FEM) simulation [25] provide a calibration for the measurement of the plate spacing. We note that changing the plate spacing shifts the resonant frequency in a predictable, almost linear fashion, at a rate of roughly 150 GHz/mm. This implies that slight changes in plate spacing (on the order of 100 μm or less) can be used to compensate for fabrication errors when designing waveguide cavities to resonate at a specific frequency.

In conclusion, this study provides a route for optimizing this waveguide-cavity geometry for sensing and spectral filtering applications. This design process may make use of the increase in Q for shallow cavities or may employ the complex behavior of the wider waveguides to probe several frequencies with a single cavity. The waveguide plate spacing may be used to fine-tune a resonance to compensate for any imperfections in the fabrication process.

This research has been supported in part by the National Science Foundation (NSF).

References

1. A. Hassani, A. Dupuis, and M. Skorobogatiy, J. Opt. Soc. Am. B **25**, 1771 (2008).
2. B. You, J.-Y. Lu, J.-H. Liou, C.-P. Yu, H.-Z. Chen, T.-A. Liu, and J.-L. Peng, Opt. Express **18**, 19353 (2010).
3. H. Kurt and D. S. Citrin, Appl. Phys. Lett. **87**, 241119 (2005).
4. A. Bingham and D. Grischkowsky, Opt. Lett. **33**, 348 (2008).
5. C. M. Yee and M. S. Sherwin, Appl. Phys. Lett. **94**, 154104 (2009).
6. M. Nagel and H. Kurz, Int. J. Infrared Millim. Waves **27**, 517 (2006).
7. M. Gerhard, C. Imhof, and R. Zengerle, J. Appl. Phys. **108**, 026102 (2010).
8. S. Yoshida, E. Kato, K. Suizu, Y. Nakagomi, Y. Ogawa, and K. Kawase, Appl. Phys. Express **2**, 012301 (2009).
9. C. Debus and P. H. Bolivar, Appl. Phys. Lett. **91**, 184102 (2007).
10. J. F. O'Hara, R. Singh, I. Brener, E. Smirnova, J. Han, A. J. Taylor, and W. Zhang, Opt. Express **16**, 1786 (2008).
11. S.-Y. Chiam, R. Singh, J. Gu, J. Han, W. Zhang, and A. A. Bettiol, Appl. Phys. Lett. **94**, 064102 (2009).
12. M. Nagel, P. H. Bolivar, and H. Kurz, Semicond. Sci. Technol. **20**, S281 (2005).
13. A. Bingham and D. Grischkowsky, Appl. Phys. Lett. **90**, 091105 (2007).
14. S. S. Harsha, N. Laman, and D. Grischkowsky, Appl. Phys. Lett. **94**, 091118 (2009).
15. R. Mendis and D. Grischkowsky, Opt. Lett. **26**, 846 (2001).
16. R. Mendis and D. M. Mittleman, J. Opt. Soc. Am. B **26**, A6 (2009).
17. R. Mendis and D. M. Mittleman, Opt. Express **17**, 14839 (2009).
18. R. Mendis, V. Astley, J. Liu, and D. M. Mittleman, Appl. Phys. Lett. **95**, 171113 (2009).
19. D. M. Mittleman, ed., *Sensing with Terahertz Radiation* (Springer, 2002).
20. T. E. Itoh, ed., *Numerical Techniques for Microwave and Millimeter-Wave Passive Structures* (Wiley, 1989).
21. F. Borsboom and H. J. Frankena, J. Opt. Soc. Am. A **12**, 1134 (1995).
22. T. Thumvongskul and T. Shiozawa, Microw. Opt. Technol. Lett. **32**, 414 (2002).
23. A. Bingham, "Propagation through THz waveguides with photonic crystal boundaries," Ph.D. dissertation (Oklahoma State University, 2007).
24. Y.-H. Liu and H.-F. Li, Nucl. Instrum. Methods **598**, 605 (2009).
25. J. Deibel, M. Escarra, N. Berndsen, K. Wang, and D. M. Mittleman, Proc. IEEE **95**, 1624 (2007).